



Provably Stable and High-Order Accurate Multi-Block Finite Difference Discretisation for Incompressible Flow

David Niemelä¹ · Gustav Eriksson¹ · Ken Mattsson¹

Received: 19 August 2025 / Revised: 23 February 2026 / Accepted: 1 March 2026
© The Author(s) 2026

Abstract

In this paper, we solve the velocity-pressure formulation of the incompressible Navier-Stokes equations by utilizing high-order finite difference operators that satisfy a summation-by-parts property on multi-block curvilinear domain discretizations. We apply the projection method to connect the interior multi-block interfaces, and we show the stability of the discretization through a discrete version of the energy method. Analytical test cases reveal that the discretization achieves good accuracy and high-order convergence. We also explore the efficiency of increasing the discretization order, showing that, in certain instances, a higher-order discretization provides greater accuracy while using fewer degrees of freedom. Additionally, our method reaches a good agreement with benchmark data for a well-studied benchmark problem.

Keywords Summation-By-Parts · Finite differences · Incompressible Navier-Stokes · Multi-block · SBP-Projection · Pressure Poisson · High-order · Velocity-Pressure

Mathematics Subject Classification 65M06

1 Introduction

The incompressible Navier-Stokes equations have been solved by numerical methods for decades, as they are of key importance in computational fluid dynamics (CFD). Among the most popular methods are *fractional step projection methods* [1], which, when used together with *staggered grids* [2], have seen much success in the past. These methods, however, exhibit some issues with boundary conditions and temporal accuracy. More recent methods include *discontinuous Galerkin methods* (DG) [3, 4] and the *finite volume method* (FV). The DG method can be constructed to be high-order accurate and handle complicated geometry because of its inherent unstructured nature. The FV method is robust and geometrically flexible; however, it is usually restricted to at most second order. In general, high-order methods tend to be more efficient than low order methods in the sense that high-order methods are more accurate per degree of freedom. This means that for a given error tolerance, a coarser grid can be used for the computations, lowering the overall computational cost of a simulation.

✉ David Niemelä
david.niemela@it.uu.se

¹ Department of Information Technology, Uppsala University, Uppsala, Sweden

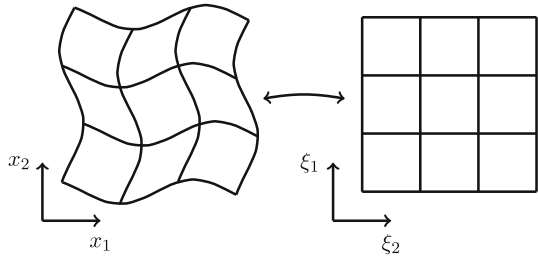
High-order methods are also often better at resolving complex flow structures such as those arising from turbulence. They do, however, come with drawbacks. More often than not, high-order methods are intricate in their construction, leading to problems with robustness and stiffness, and are often more complicated to implement for a given problem. In this study, we use high-order finite difference methods with summation-by-parts (SBP) properties [5–7]. These are essentially standard finite difference operators with special boundary closures such that the discrete operators satisfy an equivalent to the continuous integration-by-parts property. This property of the operators greatly simplifies the discrete stability analysis since many of the continuous proofs that rely on integration-by-parts can be mimicked in the discrete setting. Even though SBP finite difference operators have special boundary closures, the interior is just regular stencil-based finite differences. This has two benefits. First of all, it is relatively straightforward to construct high-order operators (in the interior using Taylor expansion analysis and for the boundary closures, typically numerical optimisation). Secondly, being based on stencil calculations, SBP finite differences are easy to implement and reap many benefits of modern computational hardware, such as GPUs for parallelisation. The operators that are used in this paper were derived in [8] and use optimised boundary closures to achieve more accurate operators.

Imposing boundary conditions using SBP finite differences is, however, non-trivial. Historically, the most common method is the simultaneous approximation term (SAT) method [9]. This method adds specifically tuned (for stability) penalisation terms to the equations to weakly enforce the imposed boundary conditions. Another method for imposing boundary conditions when using SBP schemes is the projection (P) method. This method utilises a projection operator to restrict the solutions to those where the boundary conditions are fulfilled, thus imposing the boundary conditions strongly (exactly). Both of these methods usually lead to provably stable high-order schemes [10]. Because of the inherent grid structure of finite difference methods, when dealing with complicated geometry, one needs to discretise in a curvilinear, multi-block fashion, dividing the domain into several blocks and utilising coordinate transformations. This introduces non-physical interface boundary conditions within the computational domain that must be treated stably. SBP-SAT and SBP-P schemes have proven successful when applied to complicated geometry before. See, for example [11], where the SBP-SAT method was used to solve the nonlinear Euler equations, or [12], where projection and SATs are compared in coupling multi-block domains for the wave equation.

Connections between the DG and SBP methods have been made in the past, for example, in [13], where a certain class of DG schemes was shown to be equivalent to SBP-SAT schemes. A suitable general method for solving CFD problems could be to combine the DG method close to complex objects, such as objects that are hard to model using smooth coordinate transformations, with SBP finite difference methods further away in free space. Such a coupling of the methods has been constructed before for the second order wave equation in [14]. One step towards such a method is constructing an SBP finite difference method that is able to accurately and with high-order, couple multiple curvilinear blocks, such as the method constructed in this paper.

For the CFD problem in this paper, we consider the velocity-pressure formulation of the incompressible Navier-Stokes equations in 2D, as it allows for discretisation methods with high-order accuracy and can easily be extended to 3D. The discretisation method used in this paper is the SBP-P method. It was shown in [15] that imposing Dirichlet boundary conditions, such as the common no-slip and no-penetration boundary conditions, using the projection method was more efficient at developing fine-structure phenomena in fluid flow simulations compared to the SAT method. Additionally, the strong imposition of the projection method is also useful for strictly enforcing the divergence-free criterion in the incompressible Navier-

Fig. 1 Example transformation in 2D



Stokes equations. In this work, we impose the interface boundary conditions between blocks using the projection method. The main purpose of this paper is to extend the methodology in [15] to handle complicated geometry by using curvilinear multi-block discretisations, which are, due to the projection method, stable, accurate, and high-order.

The paper is organized as follows: in Section 2, we briefly describe the coordinate transformation used for the curvilinear coordinate mappings. The summation-by-parts framework using curvilinear grids is then explained in Section 3. Furthermore, in Section 4, we present the continuous analysis of the incompressible Navier-Stokes equations, followed by the discrete analysis in Section 5. In Section 6, the numerical experiments are presented together with the results, and conclusions are drawn in Section 7.

2 Definitions

In this section, we define concepts and notations on coordinate transformations and SBP-FD methods necessary for the analysis. Throughout the paper, we use implicit summation over repeated indices, e.g., $A_i x_i = \sum_{i=0}^{N-1} A_i x_i$. Where A and x are vectors of size N .

2.1 Coordinate Transformations

We start by explaining some notations on coordinate transformations that will be used in this paper, see, for example, [16] for similar notation. Let

$$x_j = x_j(\xi_1, \dots, \xi_d), \quad j = 1, \dots, d, \tag{1}$$

be a smooth, affine transformation from a curvilinear domain Ω of dimension d , with Γ as its boundary, to a rectangular domain Ω' with boundary Γ' , see Fig. 1 for an example in 2D. Let \mathcal{J} denote the Jacobian matrix with elements $\mathcal{J}_{ij} = \partial x_j / \partial \xi_i$ and \mathcal{K} denote the matrix with elements $\mathcal{K}_{ji} = \partial \xi_i / \partial x_j$ and let $J = \det(\mathcal{J})$. We assume a one-to-one mapping, hence $J > 0$.

For functions $u, v \in \Omega$, let $(u, v)_\Omega$ denote the L^2 inner product $\int_\Omega uv \, d\Omega$ and $(u, v)_\Gamma$ denote the boundary integral $\int_\Gamma uv \, d\Gamma$. Then, the following relations hold:

$$\begin{aligned} (u, v)_\Omega &= (u, Jv)_{\Omega'}, \\ (u, v)_\Gamma &= (u, \gamma v)_{\Gamma'}, \end{aligned} \tag{2}$$

where J and γ are the surface and line element scale factors, respectively, such that $d\Omega = Jd\Omega'$ and $d\Gamma = \gamma d\Gamma'$. The outward facing normals on Γ and Γ' , denoted n_{x_j} and v_{ξ_i}

respectively, can be related through Nanson’s formula [17]:

$$n_{x_j} = \frac{J}{\gamma} \mathcal{K}_{ji} v_{\xi_i}. \tag{3}$$

To simplify the notation going forward in the paper, we will denote partial derivatives: $\frac{\partial}{\partial x_j} = \partial_{x_j}$ and $\frac{\partial}{\partial \xi_i} = \partial_{\xi_i}$. By the use of the chain rule, we can see that the derivatives on the domains are connected through:

$$\partial_{x_j} = \mathcal{K}_{ji} \partial_{\xi_i}. \tag{4}$$

A useful metric relation is

$$J \mathcal{K}_{ji} \partial_{\xi_i} = \partial_{\xi_i} J \mathcal{K}_{ji}. \tag{5}$$

With the use of (3), (4) and (5) the normal derivative on Γ' can be written as

$$\frac{\partial}{\partial n} = n_{x_j} \partial_{x_j} = v_{\xi_i} \frac{J}{\gamma} \mathcal{K}_{jl} \mathcal{K}_{jk} \partial_{\xi_k}. \tag{6}$$

2.2 Summation-By-Parts

We will briefly give an introduction to the SBP finite difference operators that are used in this paper, see for example [7] for more details. Let a one-dimensional domain Ω' be discretized by N points at nodal points $\mathbf{x} = [x_0, x_1, \dots, x_{N-1}]$. Let \mathbf{u} and \mathbf{v} be discrete functions that approximate continuous functions u and v on Ω' on the grid points.

The first and second derivative SBP operators used in this paper were first derived in [5, 18], with the following definitions:

Definition 1 A difference operator $D_1 = H^{-1}Q$ approximating $\partial/\partial x$ is a first order derivative SBP-operator if $H = H^T > 0$ and $Q + Q^T = B = \text{diag}(-1, 0, \dots, 0, 1)$.

Definition 2 Let D_1 be a first derivative SBP operator. A difference operator $D_2(c) \approx \frac{\partial}{\partial x} c(x) \frac{\partial}{\partial x}$ is said to be a compatible second derivative SBP operator, if for the norm H , the relation

$$H D_2(c) = D_1^T H \bar{c} D_1 - R(c) + B^{(c)} \hat{D}, \tag{7}$$

where $R(c) = R(c)^T \geq 0$, $\bar{c} = \text{diag}(\mathbf{c})$, where \mathbf{c} is a vector of $c(x)$ evaluated on the grid \mathbf{x} , $B^{(c)} = \text{diag}(-c_0, 0, \dots, c_{N-1})$ and \hat{D} approximates the first-derivative operator at the boundaries holds.

Using Definition 1 we see that

$$\mathbf{v}^T H D_1 \mathbf{u} = -(D_1 \mathbf{v})^T H \mathbf{u} - \mathbf{u}_0 \mathbf{v}_0 + \mathbf{u}_{N-1} \mathbf{v}_{N-1}, \tag{8}$$

which mimics the continuous integration by parts, discretely. In [19], it was shown that only diagonal-norm operators can guarantee stability for curvilinear mapped problems; therefore, we restrict our analysis to diagonal-norm SBP operators, where H is a diagonal matrix.

The 1D SBP operators can be extended from one to multiple dimensions by the use of the Kronecker product. A difference operator for dimension $\xi_i, i = 1, 2, \dots, d$, can be constructed as

$$D_{\xi_i} = I_{\xi_1} \otimes \dots \otimes I_{\xi_{i-1}} \otimes D_1 \otimes \dots \otimes I_{\xi_d} \approx \partial_{\xi_i}, \tag{9}$$

where I_{ξ_i} is the identity matrix of size $N_{\xi_i} \times N_{\xi_i}$ and N_{ξ_i} is the number of grid points in the ξ_i direction. Similarly, the multidimensional quadrature over a d -dimensional domain, Ω' , can be expressed as

$$H_{\Omega'} = H_{\xi_1} \otimes \dots \otimes H_{\xi_d}, \tag{10}$$

and the quadrature over an edge, Γ'_{ξ_i} , can be expressed as

$$H_{\Gamma'_{\xi_i}} = H_{\xi_1} \otimes \cdots \otimes H_{\xi_{i-1}} \otimes H_{\xi_{i+1}} \otimes \cdots \otimes H_{\xi_d}. \tag{11}$$

We can now express discrete inner products using the notation

$$(\mathbf{u}, \mathbf{v})_{H_{\Omega'}} = \mathbf{u}^T H_{\Omega'} \mathbf{v} \approx (u, v)_{\Omega'}, \tag{12}$$

for domain integration together with the notation

$$(\mathbf{u}, \mathbf{v})_{H_{\Gamma'}} = \sum_{\xi_i} (e_{\xi_i}^T \mathbf{u})^T H_{\Gamma'_{\xi_i}} (e_{\xi_i}^T \mathbf{v}) \approx (u, v)_{\Gamma'}, \tag{13}$$

for boundary integration, where e_{ξ_i} are restriction operators extracting the elements of \mathbf{u} and \mathbf{v} on boundary Γ'_{ξ_i} . The restriction operators are constructed as $[1, \dots, 0]$ and $[0, \dots, 1]$ on the left and right boundary, respectively, for the one-dimensional case. These can be extended to higher dimensions similarly to the SBP-operators using the Kronecker product, e.g., in two dimensions $I_N \otimes [0, \dots, 1]$.

To extend the operators to non-rectangular domains, we use the transformations defined in Section 2. Similarly to the continuous transformation, we define

$$D_{x_j} = \tilde{\mathcal{K}}_{ji} D_{\xi_j} \approx \partial_{x_j}, \tag{14}$$

where $\tilde{\mathcal{K}}_{ji}$ is a diagonal matrix that has the discretized values of \mathcal{K}_{ji} on the diagonal, approximated using the operators D_{ξ_j} on the coordinates x_j . We can also define, using the metric relation in (5),

$$\tilde{D}_{x_j} = D_{\xi_j} \tilde{\mathcal{K}}_{ji} \approx \partial_{x_j}. \tag{15}$$

Following the inner product definitions in (2) we define the SBP norms on the domain Ω and Γ as

$$\begin{aligned} H_{\Omega} &= \mathbf{J} H_{\Omega'}, \\ H_{\Gamma} &= \boldsymbol{\gamma} H_{\Gamma'}, \end{aligned} \tag{16}$$

where \mathbf{J} and $\boldsymbol{\gamma}$ are diagonal matrices with J and γ evaluated on the grid points. We can now show the SBP property of the first-derivative curvilinear SBP operators D_{x_j} and \tilde{D}_{x_j} on the domain Ω as

$$(\mathbf{v}, D_{x_j} \mathbf{u})_{H_{\Omega}} + (\tilde{D}_{x_j} \mathbf{v}, \mathbf{u})_{H_{\Omega}} = \sum_{\Gamma} (\mathbf{v}, \mathbf{u})_{H_{\Gamma}}. \tag{17}$$

Laplace operators with SBP properties on curvilinear grids have been derived on multiple occasions in the past, see, for example, [16]. An SBP Laplace operator on the domain Ω is

$$D_L = \begin{cases} D_{\xi_i \xi_j}(\alpha_{ij}) & i = j, \\ D_{\xi_i} \alpha_{ij} D_{\xi_j} & i \neq j, \end{cases} \tag{18}$$

where we define $\alpha_{ij} = \mathcal{K}_{ki} J \mathcal{K}_{kj}$. This operator satisfies the SBP property

$$(\mathbf{v}, D_L \mathbf{u})_{H_{\Omega}} = \begin{cases} -(D_{\xi_i} \mathbf{v}, \alpha_{ij} D_{\xi_j} \mathbf{u})_{H_{\Omega}} + \sum_{\Gamma} (\mathbf{v}, v_i \alpha_{ij} D_{\xi_i} \mathbf{u})_{H_{\Gamma}} - \mathbf{v}^T R_{ij} \mathbf{u}, & i = j \\ -(D_{\xi_i} \mathbf{v}, \alpha_{ij} D_{\xi_j} \mathbf{u})_{H_{\Omega}} + \sum_{\Gamma} (\mathbf{v}, v_i \alpha_{ij} D_{\xi_i} \mathbf{u})_{H_{\Gamma}}, & i \neq j, \end{cases} \tag{19}$$

which is the discrete analogue to the continuous integration by parts. The term R_{ij} is a positive definite matrix and is constructed such that $\mathbf{u}^T R_{ij} \mathbf{u} = 0$ up to the order of accuracy, see [20] for more in-depth on the construction of the matrices.

Remark 1 The Laplace operator defined in (18) makes use of the compatible second derivative SBP operators for the case $i = j$ and applies the first derivative SBP operators unto themselves for the case $i \neq j$. The analysis of the paper does not rely on the use of these compatible operators and one could apply first derivative operators unto themselves for all cases. However, the use of the compatible operators has been shown to have better numerical properties, [21].

This paper confines itself to two-dimensional problems. As such, from now on, x_1, x_2 corresponds to the physical coordinates x, y respectively, and ξ_1, ξ_2 correspond to the reference coordinates ξ, η respectively. The theory and analysis in the upcoming sections have clear extensions to three dimensions.

3 Continuous Analysis

The non-dimensional form of the incompressible Navier-Stokes equations is given by

$$\begin{aligned}
 \mathbf{V}_t &= -(\mathbf{V} \cdot \nabla) \mathbf{V} - \nabla p + \epsilon \Delta \mathbf{V}, & (x, y) \in \Omega, \quad t \geq 0, \\
 \nabla \cdot \mathbf{V} &= 0, & (x, y) \in \Omega, \quad t \geq 0, \\
 B(\mathbf{V}, p, \nabla \mathbf{V}) &= \mathbf{G}, & (x, y) \in \Gamma, \quad t \geq 0, \\
 \mathbf{V} &= \mathbf{T}, & (x, y) \in \Omega, \quad t = 0,
 \end{aligned} \tag{20}$$

where $\mathbf{V} = \begin{bmatrix} u \\ v \end{bmatrix}$ is the velocity field, p is the pressure, ϵ is the kinematic viscosity parameter, $B(\mathbf{V}, p, \nabla \mathbf{V})$ is a function defining the boundary conditions, \mathbf{G} is the boundary data, and \mathbf{T} is the initial data.

3.1 Velocity-Pressure Formulation

We refer to the form of the incompressible Navier-Stokes in (20) as the velocity-divergence formulation, as it describes the system using the velocity field \mathbf{V} and the divergence of said velocity field. The velocity-pressure formulation is found by taking the divergence of the momentum equation, the first equation in (20),

$$\nabla \cdot (\mathbf{V}_t) + \nabla \cdot (\mathbf{V} \cdot \nabla) \mathbf{V} = \nabla \cdot (-\nabla p) + \nabla \cdot (\epsilon \Delta \mathbf{V}), \tag{21}$$

and applying the divergence free condition, $\nabla \cdot \mathbf{V} = 0$, resulting in the pressure Poisson equation (PPE),

$$\Delta p = -(\partial_x u)^2 - 2\partial_y u \partial_x v - (\partial_y v)^2. \tag{22}$$

As shown in [22], boundary conditions for the divergence are required for the divergence to be non-growing in time, as well as divergence free initial data. This leads to the full velocity-pressure formulation of the incompressible Navier-Stokes equations where the divergence free condition has been replaced by the PPE together with divergence free boundary condition

and divergence free initial condition. The resulting form of the equations are

$$\begin{aligned}
 \mathbf{V}_t &= -(\mathbf{V} \cdot \nabla) \mathbf{V} - \nabla p + \epsilon \Delta \mathbf{V}, & (x, y) \in \Omega, \quad t \geq 0, \\
 \Delta p &= -(\partial_x u)^2 - 2\partial_y u \partial_x v - (\partial_y v)^2. & (x, y) \in \Omega, \quad t \geq 0, \\
 \nabla \cdot \mathbf{V} &= 0, & (x, y) \in \Gamma, \quad t \geq 0, \\
 B(\mathbf{V}, p) &= \mathbf{G} & (x, y) \in \Gamma, \quad t \geq 0, \\
 \mathbf{V} &= \mathbf{T}, & (x, y) \in \Omega, \quad t = 0, \\
 \nabla \cdot \mathbf{V} &= 0, & (x, y) \in \Omega, \quad t = 0.
 \end{aligned} \tag{23}$$

3.2 Energy Analysis

Taking the L^2 inner product of the momentum equation, first row in (23), with \mathbf{V} ,

$$(\mathbf{V}, \mathbf{V}_t)_\Omega = (\mathbf{V}, -(\mathbf{V} \cdot \nabla) \mathbf{V} - \nabla p + \epsilon \Delta \mathbf{V})_\Omega, \tag{24}$$

and grouping the terms with u and v ,

$$\begin{aligned}
 (u, \partial_t u)_\Omega + (v, \partial_t v)_\Omega &= -(u, u(\partial_x u) + v(\partial_y u) + \partial_x p)_\Omega - (v, u(\partial_x v) + v(\partial_y v) + \partial_y p)_\Omega \\
 &\quad + \epsilon(u, \Delta u)_\Omega + \epsilon(v, \Delta v)_\Omega.
 \end{aligned} \tag{25}$$

Then, with the use of the following identity for smooth functions $a(x)$ and $b(x)$:

$$a \partial_x b = \frac{1}{2}(a \partial_x b + \partial_x(ab) - \partial_x ab) \tag{26}$$

for the nonlinear advection terms, noting $u \partial_x u = \partial_x uu$ and $v \partial_y v = \partial_y vv$. We can show using integration by parts that

$$\frac{d}{dt} (\|u\|_\Omega^2 + \|v\|_\Omega^2) + 2\epsilon (\|\nabla u\|_\Omega^2 + \|\nabla v\|_\Omega^2) = BT + RT. \tag{27}$$

On the left hand side we have the energy term, which is the norm of the velocity field, and the viscous dissipation term, which is the norm of the gradient of the velocity field. On the right hand side we group the remaining terms as BT , *boundary terms*, that are

$$BT = - \int_\Gamma (u^2 + v^2 + 2p) (un_x + vn_y) + 2\epsilon \left(u \frac{\partial u}{\partial n} + v \frac{\partial v}{\partial n} \right) ds \tag{28}$$

and RT , *remainder term*, which is an indefinite inner product term containing the divergence of the solution:

$$RT = (2p + u^2 + v^2, \nabla \cdot \mathbf{V})_\Omega. \tag{29}$$

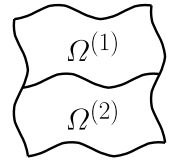
The energy equation (27) shows that the energy, given by $\|u\|_\Omega^2 + \|v\|_\Omega^2$, is bounded and decreasing if the boundary terms are handled correctly such that $BT \leq 0$, and if the divergence of the solution is zero, such that $RT = 0$.

The boundary terms, BT , can be written in the following way [22]:

$$BT = - \int_\Gamma w^T A w \, d\Gamma, \tag{30}$$

where

Fig. 2 Example of multi-block domain consisting of two blocks, $\Omega^{(1)}$ and $\Omega^{(2)}$ sharing an interface



$$w = \begin{bmatrix} u \\ v \\ p \\ \epsilon \frac{\partial u}{\partial n} \\ \epsilon \frac{\partial v}{\partial n} \end{bmatrix} \text{ and } A = \begin{bmatrix} w_\lambda & 0 & n_x & -1 & 0 \\ 0 & w_\lambda & n_y & 0 & -1 \\ n_x & n_y & 0 & 0 & 0 \\ -1 & 0 & 0 & 0 & 0 \\ 0 & -1 & 0 & 0 & 0 \end{bmatrix}. \tag{31}$$

Here $w_\lambda = un_x + vn_y$, is the normal velocity, and $w_\tau = un_y - vn_x$ is the tangential velocity.

In this paper, we prescribe Dirichlet boundary conditions at no-slip and inflow boundaries, and characteristic boundary conditions (CBC) at outflow boundaries. Energy estimates when using Dirichlet boundary conditions are easily obtained. Assuming divergence-free velocity field, $\nabla \cdot \mathbf{V} = 0$ and homogeneous boundary conditions, $\mathbf{G} = 0$, leads to $BT = 0$ and $RT = 0$, giving the energy estimate

$$\frac{d}{dt} (\|u\|_\Omega^2 + \|v\|_\Omega^2) + 2\epsilon (\|\nabla u\|_\Omega^2 + \|\nabla v\|_\Omega^2) = 0. \tag{32}$$

With the purpose of being concise, in this paper, we will only present the idea and the stability result for the CBC. Details on the derivations can be found in [22]. They were also used in [15] as outflow boundary conditions. The idea of the CBC is such that $w^T A w \geq 0$. By diagonalising the matrix A and using the signs of the eigenvalues λ we find that the following are the characteristic boundary conditions:

$$\begin{aligned} C_2 &= \lambda_2 w_\tau - n_y \epsilon \frac{\partial u}{\partial n} + n_x \epsilon \frac{\partial v}{\partial n} = 0, \\ C_4 &= -\lambda_4 w_\lambda - p + n_x \epsilon \frac{\partial u}{\partial n} + n_y \epsilon \frac{\partial v}{\partial n} = 0, \end{aligned} \tag{33}$$

where

$$\begin{aligned} \lambda_2 &= \frac{w_\lambda - \sqrt{w_\lambda^2 + 4}}{2}, \\ \lambda_4 &= \frac{w_\lambda - \sqrt{w_\lambda^2 + 8}}{2}. \end{aligned} \tag{34}$$

These conditions guarantee that the boundary terms stay negative and only contribute with dissipation to the energy. Together with a divergence-free velocity field this means that we can show

$$\frac{d}{dt} (\|u\|_\Omega^2 + \|v\|_\Omega^2) + 2\epsilon (\|\nabla u\|_\Omega^2 + \|\nabla v\|_\Omega^2) \leq 0, \tag{35}$$

ensuring stability of the scheme.

3.2.1 Multi-Block Energy Analysis

Now we turn to the analysis of a multi-block domain. Here we will illustrate the analysis using a simple example, the two block domain seen in Fig. 2. The analysis can easily be generalised to more complex domains.

Let the superscripts (1) and (2) denote the blocks of the multi-block domain defined by $\Omega = \Omega^{(1)} \cup \Omega^{(2)}$ with the interface $\Gamma_I = \Omega^{(1)} \cap \Omega^{(2)}$, see Fig. 2. By deriving the energy equations (27) for both blocks and summing the resulting terms, assuming the outer boundary terms (the terms BT) are taken care of by suitable boundary conditions, Dirichlet for example, we obtain the following energy equation for the full domain:

$$\begin{aligned} \frac{d}{dt} & \left(\|u^{(1)}\|_{\Omega^{(1)}}^2 + \|v^{(1)}\|_{\Omega^{(1)}}^2 + \|u^{(2)}\|_{\Omega^{(2)}}^2 + \|v^{(2)}\|_{\Omega^{(2)}}^2 \right) \\ & + 2\epsilon \left(\|\nabla u^{(1)}\|_{\Omega^{(1)}}^2 + \|\nabla v^{(1)}\|_{\Omega^{(1)}}^2 + \|\nabla u^{(2)}\|_{\Omega^{(2)}}^2 + \|\nabla v^{(2)}\|_{\Omega^{(2)}}^2 \right) = RT^{(1)} + RT^{(2)} + IT, \end{aligned} \tag{36}$$

where the terms $RT^{(1)}$ and $RT^{(2)}$ are given in (29) for the two blocks. The term IT , the *interface terms*, corresponding to the boundary Γ_I , for both block discretisations are given by

$$\begin{aligned} IT = & - \left(u^{(1)}u^{(1)} + v^{(1)}v^{(1)} + 2p^{(1)}, n_x^{(1)}u^{(1)} + n_y^{(1)}v^{(1)} \right)_{\Gamma_I} \\ & + 2\epsilon \left(\left(u^{(1)}, \frac{\partial u^{(1)}}{\partial n^{(1)}} \right)_{\Gamma_I} + \left(v^{(1)}, \frac{\partial v^{(1)}}{\partial n^{(1)}} \right)_{\Gamma_I} \right) \\ & - \left(u^{(2)}u^{(2)} + v^{(2)}v^{(2)} + 2p^{(2)}, n_x^{(2)}u^{(2)} + n_y^{(2)}v^{(2)} \right)_{\Gamma_I} \\ & + 2\epsilon \left(\left(u^{(2)}, \frac{\partial u^{(2)}}{\partial n^{(2)}} \right)_{\Gamma_I} + \left(v^{(2)}, \frac{\partial v^{(2)}}{\partial n^{(2)}} \right)_{\Gamma_I} \right). \end{aligned} \tag{37}$$

If we impose continuity for $p, u, v, \frac{\partial u}{\partial n}$, and $\frac{\partial v}{\partial n}$ over the interfaces, i.e for $(x, y) \in \Gamma_I$:

$$\begin{aligned} p^{(1)} &= p^{(2)}, \quad u^{(1)} = u^{(2)}, \quad v^{(1)} = v^{(2)}, \\ \frac{\partial u^{(1)}}{\partial n} &= \frac{\partial u^{(2)}}{\partial n}, \quad \frac{\partial v^{(1)}}{\partial n} = \frac{\partial v^{(2)}}{\partial n}, \end{aligned} \tag{38}$$

then $IT = 0$, since the normals, $n^{(1)}$ and $n^{(2)}$, are antiparallel. With this, we arrive at an energy estimate for the multi-block discretisations similar to that of the single block energy estimate. Meaning that we have a bounded and decreasing energy for the multi-block system. The analysis for more blocks follows easily from this.

Remark 2 It should be noted that the estimates derived in this section are not, by themselves, a proof of nonlinear well-posedness for the incompressible Navier-Stokes equations. Nonlinear well-posedness is typically established via linearisation and localisation arguments; see, for example [23]. Nevertheless, assuming sufficient smoothness of the underlying solution, the nonlinear energy estimate obtained here directly yields an energy estimate for the corresponding linearised problem. The analysis of the nonlinear problem with non-homogeneous boundary conditions is non-trivial and is beyond the scope of the present paper. We refer the reader to [24, 25] for such analysis.

4 Discrete Analysis

We will now turn to the discretisation, showing the construction and stability of the scheme. We spatially discretize the system (23) by using SBP operators. As an illustrative example, we discretize the two block domain shown in Fig. 2 by constructing a multi-block grid of $N \times N$ grid points in each block, where N is the number of grid points per dimension. We keep to this simple case for brevity of the notation, but the methodology easily extends to different grid sizes in each block as well as dimensions. The spatially discretized system is given by

$$\begin{aligned}
 \mathbf{V}_t &= D(\mathbf{V}, \mathbf{p}), & t \geq 0, \\
 D_L \mathbf{p} &= F, & t \geq 0, \\
 L_m \mathbf{V} &= \mathbf{g}_m, & t \geq 0, \\
 L_p \mathbf{p} &= \mathbf{g}_p, & t \geq 0, \\
 \mathbf{V} &= \mathbf{V}_0, & t = 0,
 \end{aligned}
 \tag{39}$$

where $\mathbf{V} = [\mathbf{V}^{(1)}, \mathbf{V}^{(2)}]^T$, $\mathbf{V}^{(1)} = [\mathbf{u}^{(1)}, \mathbf{v}^{(1)}]^T$ and $\mathbf{V}^{(2)} = [\mathbf{u}^{(2)}, \mathbf{v}^{(2)}]^T$. The superscripts correspond to variables connected to that numbered block. In order to reduce notation, the derivative operators will be assumed to correspond to the same block as the vector it is connected to, e.g. $D_x \mathbf{u}^{(1)} = D_x^{(1)} \mathbf{u}^{(1)}$. The operators L_m and L_p are the boundary operators for the momentum and pressure equations, respectively, defined by discretising the continuous boundary conditions, the exact form of which depends on the problem at hand. The vectors \mathbf{g}_m and \mathbf{g}_p are the boundary data for the momentum and pressure equations, respectively. The vector \mathbf{V}_0 is the given initial data for the velocity. The right-hand side of the momentum equation is given by

$$D(\mathbf{V}, \mathbf{p}) = \begin{bmatrix} (-D_x^{(s)} - D_y^{(s)} + \epsilon D_L) \mathbf{u}^{(1)} - D_x \mathbf{p}^{(1)} \\ (-D_x^{(s)} - D_y^{(s)} + \epsilon D_L) \mathbf{v}^{(1)} - D_y \mathbf{p}^{(1)} \\ (-D_x^{(s)} - D_y^{(s)} + \epsilon D_L) \mathbf{u}^{(2)} - D_x \mathbf{p}^{(2)} \\ (-D_x^{(s)} - D_y^{(s)} + \epsilon D_L) \mathbf{v}^{(2)} - D_y \mathbf{p}^{(2)} \end{bmatrix}. \tag{40}$$

where the operators in (40) are

$$D_x^{(s)}(\mathbf{u}) = \frac{1}{2} (U \tilde{D}_x + D_x U - U_x) \quad \text{and} \quad D_y^{(s)}(\mathbf{v}) = \frac{1}{2} (V \tilde{D}_y + D_y V - V_y). \tag{41}$$

These are skew-symmetric split advection operators using the definition of (14) and (15) for D_x , D_y and \tilde{D}_x , \tilde{D}_y respectively. The U and U_x are diagonal matrices with entries \mathbf{u} and $\tilde{D}_x \mathbf{u}$ respectively, and equivalently for V and V_y . For the pressure Poisson equation, the second row in (39), the right-hand side is given by

$$F = -U_x (D_x \mathbf{u}) - 2U_y (D_x \mathbf{v}) - V_y (D_y \mathbf{v}). \tag{42}$$

To impose the boundary conditions, we use the projection method. For more details on the projection method, see, for example, [26] where the projection was first introduced. The projection operator P is constructed such that it projects the solution so that the boundary conditions, defined by the operator L , are fulfilled. For stability, P is also constructed such that it is self-adjoint with respect to the discrete inner product, H . Fulfilling these criteria results in

$$P = I - H^{-1} L^T (L H^{-1} L^T)^{-1} L. \tag{43}$$

We then construct operators P_m, P_p that are projection operators to impose boundary conditions for the momentum and pressure equation respectively, using the boundary condition operators L_m and L_p .

The boundary condition operators L_m and L_p together with the boundary data \mathbf{g}_m and \mathbf{g}_p are constructed as:

$$L_m = \begin{bmatrix} L_m^{(1)} & \mathbf{0} \\ \mathbf{0} & L_m^{(2)} \\ & L_{mI} \end{bmatrix}, \text{ with data } \mathbf{g}_{(m)} = \begin{bmatrix} \mathbf{g}_{(m)e,w,n}^{(1)} \\ \mathbf{g}_{(m)e,w,s}^{(2)} \\ \mathbf{0} \end{bmatrix}, \tag{44}$$

and

$$L_p = \begin{bmatrix} L_p^{(1)} & \mathbf{0} \\ \mathbf{0} & L_p^{(2)} \\ & L_{pI} \end{bmatrix}, \text{ with data } \mathbf{g}_{(p)} = \begin{bmatrix} \mathbf{g}_{(p)e,w,n}^{(1)} \\ \mathbf{g}_{(p)e,w,s}^{(2)} \\ \mathbf{0} \end{bmatrix}. \tag{45}$$

The operators $L_{m/p}^{(1)}$ and $L_{m/p}^{(2)}$ handle the outer boundary conditions for the first and second block respectively, while $L_{mI/pI}$ handles the interface conditions between the blocks. Here we focus on the part concerning the interface conditions. We assume that the outer boundaries are handled in a stable manner, as in [15] where the projection method is used for the one block case. For the momentum equations, L_{mI} is constructed as

$$L_{mI} = \begin{bmatrix} e_s^{(1)} & \mathbf{0} & -e_n^{(2)} & \mathbf{0} \\ \mathbf{0} & e_s^{(1)} & \mathbf{0} & -e_n^{(2)} \\ e_s^{(1)} D_x & \mathbf{0} & -e_n^{(2)} D_x & \mathbf{0} \\ \mathbf{0} & e_s^{(1)} D_y & \mathbf{0} & -e_n^{(2)} D_y \end{bmatrix}. \tag{46}$$

Where $e_s^{(1)}, e_n^{(2)}$ are restriction operators, extracting the values on the boundaries to the south and north (up and down) respectively, for each block. The boundary operator (46) corresponds to imposing the continuity that we found in (38) for the velocities. The pressure boundary operator for the interface is constructed in the following way:

$$L_{pI} = \begin{bmatrix} e_s^{(1)} & -e_n^{(2)} \\ e_s^{(1)} & -e_n^{(2)} \\ e_s^{(1)} D_x & -e_n^{(2)} D_x \\ e_s^{(1)} D_y & -e_n^{(2)} D_y \end{bmatrix}. \tag{47}$$

This ensures continuity of the pressure and the normal derivative of the pressure on the interface, required from the continuity conditions (38), and the PPE. With the projection operators P_m and P_p , constructed using L_m and L_p , we can now impose the boundary conditions on our discretisation and write the scheme

$$\begin{aligned} \mathbf{V}_t &= P_m D(\hat{\mathbf{V}}, \mathbf{p}) + (I - P_m)\tilde{\mathbf{g}}_{(m)t}, & t \geq 0 \\ HP_p D_L(P_p \mathbf{p} + (I - P_p)\tilde{\mathbf{g}}_{(p)}) - \sigma H(I - P_p)(\mathbf{p} - \tilde{\mathbf{g}}_{(p)t}) &= HP_p F, & t \geq 0 \\ \mathbf{V} &= \mathbf{V}_0, & t = 0. \end{aligned} \tag{48}$$

Where $\hat{\mathbf{V}} = P_m \mathbf{V} - (I - P_m)\tilde{\mathbf{g}}_m$. The term $\sigma H(I - P_p)(\mathbf{p} - \tilde{\mathbf{g}}_{(p)t})$ is a term necessary to remove a zero eigenvalue introduced to the problem from the projection operator, see [27]. In the computations we use $\sigma = 1/h^2$, h being the distance between grid points.

Remark 3 The value of σ should be proportional to $1/h^2$. We have done extensive numerical testing and found that that when varying the scaling factor C , $\sigma = C/h^2$, between 10^{-2} and 10^6 the iterations of the PPE solver is decreased for larger values of C . There is most likely a sweet spot, or interval, for the value of C that minimizes the number of iterations required for the PPE, but we have not found it. The difference was not large enough to warrant further investigation.

Lemma 1 *Assuming that the outer boundary conditions are implemented in a stable manner, the SBP-P scheme (48) is a stable approximation to (23).*

Proof We prove stability of the scheme using the energy method. Assuming $\mathbf{g}_m = 0$ and taking the inner product of the momentum equation with \mathbf{V} ,

$$(\mathbf{V}, \mathbf{V}_t)_{\bar{H}_\Omega} = (\mathbf{V}, P_m D (\hat{\mathbf{V}}, \mathbf{p}))_{\bar{H}_\Omega}, \tag{49}$$

where $\bar{H}_\Omega = H_\Omega \otimes I_2$. Using $\bar{H}_\Omega P_m = P_m \bar{H}_\Omega$, expanding the operator D , and similarly to the continuous case grouping the terms with \mathbf{u} and \mathbf{v} gives

$$\begin{aligned} & (\mathbf{u}^{(1)}, \mathbf{u}_t^{(1)})_{H_\Omega} + (\mathbf{v}^{(1)}, \mathbf{v}_t^{(1)})_{H_\Omega} \\ & + (\mathbf{u}^{(2)}, \mathbf{u}_t^{(2)})_{H_\Omega} + (\mathbf{v}^{(2)}, \mathbf{v}_t^{(2)})_{H_\Omega} = - \left(\hat{\mathbf{u}}^{(1)}, D_x^{(s)} \hat{\mathbf{u}}^{(1)} + D_y^{(s)} \hat{\mathbf{u}}^{(1)} + D_x \mathbf{p}^{(1)} \right)_{H_\Omega} \\ & \quad - \left(\hat{\mathbf{v}}^{(1)}, D_x^{(s)} \hat{\mathbf{v}}^{(1)} + D_y^{(s)} \hat{\mathbf{v}}^{(1)} + D_y \mathbf{p}^{(1)} \right)_{H_\Omega} \\ & \quad - \left(\hat{\mathbf{u}}^{(2)}, D_x^{(s)} \hat{\mathbf{u}}^{(2)} + D_y^{(s)} \hat{\mathbf{u}}^{(2)} + D_x \mathbf{p}^{(2)} \right)_{H_\Omega} \\ & \quad - \left(\hat{\mathbf{v}}^{(2)}, D_x^{(s)} \hat{\mathbf{v}}^{(2)} + D_y^{(s)} \hat{\mathbf{v}}^{(2)} + D_y \mathbf{p}^{(2)} \right)_{H_\Omega} \\ & \quad + \epsilon \left(\hat{\mathbf{u}}^{(1)}, D_L \hat{\mathbf{u}}^{(1)} \right)_{H_\Omega} + \epsilon \left(\hat{\mathbf{v}}^{(1)}, D_L \hat{\mathbf{v}}^{(1)} \right)_{H_\Omega} \\ & \quad + \epsilon \left(\hat{\mathbf{u}}^{(2)}, D_L \hat{\mathbf{u}}^{(2)} \right)_{H_\Omega} + \epsilon \left(\hat{\mathbf{v}}^{(2)}, D_L \hat{\mathbf{v}}^{(2)} \right)_{H_\Omega}. \end{aligned} \tag{50}$$

Applying the skew-symmetry (41) to the advection terms, and using the SBP property of the operators, again assuming the outer boundaries are handled stably, we can show that

$$\frac{d}{dt} (E^{(1)} + E^{(2)}) + DI^{(1)} + DI^{(2)} = RT^{(1)} + RT^{(2)} + IT, \tag{51}$$

where

$$\begin{aligned} E^{(1,2)} &= \|\mathbf{u}^{(1,2)}\|_{H_\Omega^{(1,2)}}^2 + \|\mathbf{v}^{(1,2)}\|_{H_\Omega^{(1,2)}}^2, \\ DI^{(1,2)} &= 2\epsilon \left((\tilde{D}_x \hat{\mathbf{u}}^{(1,2)}, D_x \hat{\mathbf{u}}^{(1,2)})_{H_\Omega^{(1,2)}} + (\tilde{D}_y \hat{\mathbf{u}}^{(1,2)}, D_y \hat{\mathbf{u}}^{(1,2)})_{H_\Omega^{(1,2)}} \right) \\ & \quad + 2\epsilon \left((\tilde{D}_x \hat{\mathbf{v}}^{(1,2)}, D_x \hat{\mathbf{v}}^{(1,2)})_{H_\Omega^{(1,2)}} + (\tilde{D}_y \hat{\mathbf{v}}^{(1,2)}, D_y \hat{\mathbf{v}}^{(1,2)})_{H_\Omega^{(1,2)}} \right) \\ & \quad + \hat{\mathbf{u}}^{(1,2)T} R_L \hat{\mathbf{u}}^{(1,2)} + \hat{\mathbf{v}}^{(1,2)T} R_L \hat{\mathbf{v}}^{(1,2)} \\ RT^{(1,2)} &= \left(\hat{\mathbf{u}}^{(1,2)}, (\bar{\mathbf{u}}_x^{(1,2)} + \bar{\mathbf{v}}_y^{(1,2)}) \hat{\mathbf{u}}^{(1,2)} \right)_{H_\Omega^{(1,2)}} \\ & \quad + 2(D_x \hat{\mathbf{u}}^{(1,2)} + D_y \hat{\mathbf{v}}^{(1,2)}, \mathbf{p}^{(1,2)})_{H_\Omega} \\ & \quad + \left(\hat{\mathbf{v}}^{(1,2)}, (\bar{\mathbf{u}}_x^{(1,2)} + \bar{\mathbf{v}}_y^{(1,2)}) \hat{\mathbf{v}}^{(1,2)} \right)_{H_\Omega^{(1,2)}} \end{aligned} \tag{52}$$

and

$$\begin{aligned}
 IT = & - \left(\bar{\mathbf{u}}^{(1)} \hat{\mathbf{u}}^{(1)}, \hat{\mathbf{u}}^{(1)} \right)_{H\Gamma_I} - \left(\bar{\mathbf{v}}^{(1)} \hat{\mathbf{v}}^{(1)}, \hat{\mathbf{v}}^{(1)} \right)_{H\Gamma_I} + 2 \left(\hat{\mathbf{u}}^{(1)}, \mathbf{p}^{(1)} \right)_{H\Gamma_I} \\
 & + 2\epsilon \left(\left(\hat{\mathbf{u}}^{(1)}, n_x^{(1)} D_x \hat{\mathbf{u}}^{(1)} \right)_{H\Gamma_I} + \left(\hat{\mathbf{u}}^{(1)}, n_y^{(1)} D_y \hat{\mathbf{u}}^{(1)} \right)_{H\Gamma_I} \right) \\
 & - \left(\bar{\mathbf{u}}^{(1)} \hat{\mathbf{v}}^{(1)}, \hat{\mathbf{v}}^{(1)} \right)_{H\Gamma_I} - \left(\bar{\mathbf{v}}^{(1)} \hat{\mathbf{u}}^{(1)}, \hat{\mathbf{u}}^{(1)} \right)_{H\Gamma_I} + 2 \left(\hat{\mathbf{v}}^{(1)}, \mathbf{p}^{(1)} \right)_{H\Gamma_I} \\
 & + 2\epsilon \left(\left(\hat{\mathbf{v}}^{(1)}, n_x^{(1)} D_x \hat{\mathbf{v}}^{(1)} \right)_{H\Gamma_I} + 2 \left(\hat{\mathbf{v}}^{(1)}, n_y^{(1)} D_y \hat{\mathbf{v}}^{(1)} \right)_{H\Gamma_I} \right) \\
 & + \left(\bar{\mathbf{u}}^{(2)} \hat{\mathbf{u}}^{(2)}, \hat{\mathbf{u}}^{(2)} \right)_{H\Gamma_I} + \left(\bar{\mathbf{v}}^{(2)} \hat{\mathbf{v}}^{(2)}, \hat{\mathbf{v}}^{(2)} \right)_{H\Gamma_I} - 2 \left(\hat{\mathbf{u}}^{(2)}, \mathbf{p}^{(2)} \right)_{H\Gamma_I} \\
 & - 2\epsilon \left(\left(\hat{\mathbf{u}}^{(2)}, n_x^{(2)} D_x \hat{\mathbf{u}}^{(2)} \right)_{H\Gamma_I} - \left(\hat{\mathbf{u}}^{(2)}, n_y^{(2)} D_y \hat{\mathbf{u}}^{(2)} \right)_{H\Gamma_I} \right) \\
 & + \left(\bar{\mathbf{u}}^{(2)} \hat{\mathbf{v}}^{(2)}, \hat{\mathbf{v}}^{(2)} \right)_{H\Gamma_I} + \left(\bar{\mathbf{v}}^{(2)} \hat{\mathbf{u}}^{(2)}, \hat{\mathbf{u}}^{(2)} \right)_{H\Gamma_I} - 2 \left(\hat{\mathbf{v}}^{(2)}, \mathbf{p}^{(2)} \right)_{H\Gamma_I} \\
 & - 2\epsilon \left(\left(\hat{\mathbf{v}}^{(2)}, n_x^{(2)} D_x \hat{\mathbf{v}}^{(2)} \right)_{H\Gamma_I} - 2 \left(\hat{\mathbf{v}}^{(2)}, n_y^{(2)} D_y \hat{\mathbf{v}}^{(2)} \right)_{H\Gamma_I} \right).
 \end{aligned} \tag{53}$$

Since $L_m \mathbf{V} = L_m P_m \mathbf{V} = 0$ and $L_p \mathbf{p} = L_p P_p \mathbf{p} = 0$ and by the definition of P_m and P_p , we have that

$$\begin{aligned}
 \hat{\mathbf{u}}^{(1)} &= \hat{\mathbf{u}}^{(2)}, \quad \hat{\mathbf{v}}^{(1)} = \hat{\mathbf{v}}^{(2)}, \quad D_x \hat{\mathbf{u}}^{(1)} = D_x \hat{\mathbf{u}}^{(2)}, \\
 D_y \hat{\mathbf{v}}^{(1)} &= D_y \hat{\mathbf{v}}^{(2)}, \quad \text{and } \mathbf{p}^{(1)} = \mathbf{p}^{(2)}
 \end{aligned} \tag{54}$$

on Γ_I , meaning the term $IT = 0$. The $\bar{\mathbf{u}}, \bar{\mathbf{v}}$ are here diagonal matrices with $\hat{\mathbf{u}}, \hat{\mathbf{v}}$, respectively, on the diagonal. As shown in [15], the discrete divergence is zero if the initial data is divergence free, meaning $RT = 0$. This leads to the energy estimate

$$\frac{d}{dt} (E^{(1)} + E^{(2)}) = -DI^{(1)} - DI^{(2)} \leq 0, \tag{55}$$

which is a discrete equivalent to the continuous energy estimate, proving stability of (39). \square

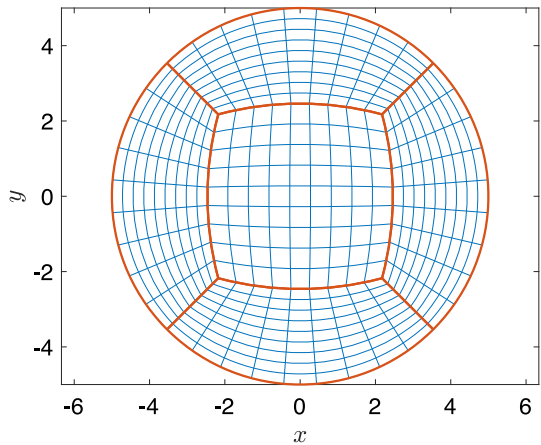
The skew symmetry and the summation by parts property mean we can mimic the continuous energy method discretely step-by-step, replacing integration by parts with summation by parts and cancelling the skew symmetric terms. Thus, ensuring we reach the same estimate discretely as we did for the continuous case.

We can now use the system of ODEs (48) to compute the solution. The pressure in the momentum equations is, in essence, replaced by the linear system of equations given by the PPE, fully given by the momentum variables \mathbf{u}, \mathbf{v} .

5 Numerical Experiments

To verify the convergence and accuracy of the discretisation, two problems are considered. First, we solve the analytic Taylor-Green vortex problem to show the convergence of the schemes. The second problem is a well-studied benchmark problem for incompressible flow, the flow around a cylinder [28]. The PPE system is solved using the iterative conjugate gradient method, as implemented by the Matlab command *pcg*, with an error tolerance of 10^{-9} , with modified incomplete Cholesky preconditioning with a drop tolerance of 10^{-10} .

Fig. 3 Multi-block domain consisting of 5 blocks used to discretise a circle. Red lines indicate the boundaries of blocks and blue lines indicate the gridlines in each block



For time integration, the classical 4th order Runge-Kutta method is used with timestep $\Delta t \propto \epsilon h^2$, meaning proportional to the spatial discretisation step-size squared times the viscosity coefficient, ϵ , for the given problem. The time-step is chosen small enough so that the temporal errors are negligible compared to the spatial errors. For the tests, we use the boundary optimised SBP operators derived in [8].

5.1 Taylor-Green Vortex Problem

The Taylor-Green vortex problem has an analytical solution given by

$$\begin{aligned}
 u &= -\cos(\alpha) \sin(\beta) \exp(-2\pi^2 \epsilon t) + u_\infty \cos(\theta), \\
 v &= \sin(\alpha) \cos(\beta) \exp(-2\pi^2 \epsilon t) + u_\infty \sin(\theta), \\
 p &= -\frac{1}{4} (\cos(2\alpha) + \cos(2\beta)) \exp(-4\pi^2 \epsilon t), \\
 \alpha &= \pi (x - u_\infty \cos(\theta)t), \quad \beta = \pi (y - u_\infty \sin(\theta)t),
 \end{aligned}
 \tag{56}$$

in two dimensions. Here u_∞ is the speed of the vortices, and θ is the angle at which they move. We use the analytic solution as the boundary and initial data with the parameters $\theta = \pi/3$ and $\epsilon = 0.01$. The errors are measured in the H -norm, (12), of the difference between the analytic and approximate solutions. We solve the problem on the circular domain shown in Fig. 3.

In Fig. 4 we show a snapshot plot of the pressure as well as the error using a 10th order operator with 51005 grid points at time $T = 2$. One can clearly see where the interfaces between the blocks are, as the error is higher there due to the decreased accuracy of the boundary stencils in the SBP operators.

In Fig. 5 the error in velocity and pressure is plotted against the number of degrees of freedom for the Taylor-Green vortex problem using operators of order 6, 8, 10, and 12, denoted by the order of the interior stencil. The operator’s boundary closures are of lower order than the interior stencil. The operators used in this paper of order p have a boundary closure of order $p/2 - 1$ [8], without affecting the overall convergence rate of the scheme [29]. Theoretical rate of convergence for linear incompletely parabolic problems for the operators used is limited to $\min(p, p/2 + 1)$ [30]. While this is not the exact type of problem considered herein, it can

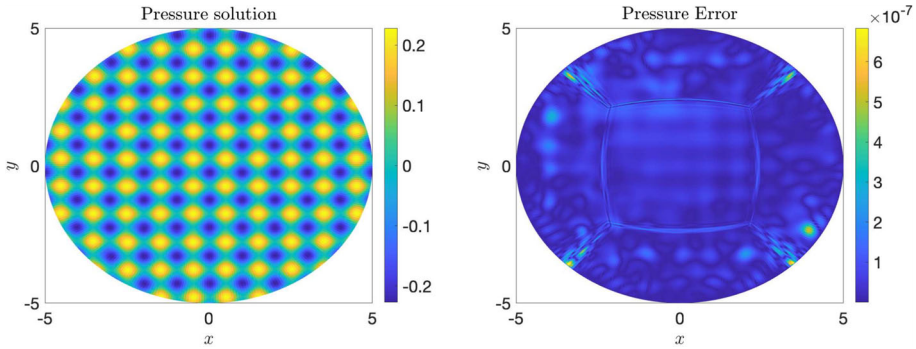


Fig. 4 Solution of the pressure field and the magnitude of the error of the 10th order scheme on a circular multi-block domain at time $T = 2$ with 51005 grid points

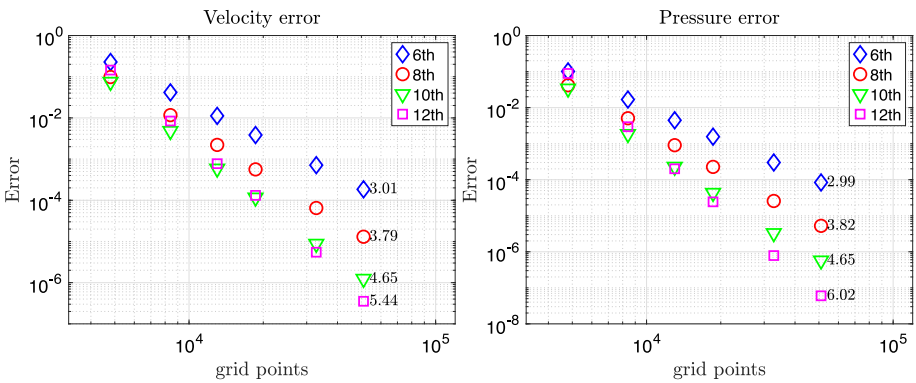


Fig. 5 Convergence for the velocity and pressure for a multi-block circular domain for the Taylor-Green vortex problem

serve as a guideline to what might be expected. The results in Fig. 5 show convergence rates that are $p/2$. One can assume that the coupling with the pressure equation, the non-linearities, and the curvilinear grids have an impact on the order of convergence. The use of multi-block domains also increases the impact of the boundary closures. The results still clearly show high-order convergence of the discretisation in both pressure and velocity.

The results from the Taylor-Green vortex problem also show an increase in efficiency as we increase the order of the scheme. For example, the 10th order shows a significant decrease in degrees of freedom (DOF) for the same error compared to the 6th and 8th order schemes, while staying on par with the 12th order scheme until the end. To further investigate the efficiency increase, Fig. 6 shows the error against the runtime, measuring efficiency as time to solution for a given error. To give the schemes a fairer comparison, the time-step was chosen as roughly 1/2 of an experimentally found, stable limit for each of the schemes. From the results, it can be seen that the efficiency of the schemes tends to increase with the order of the scheme. The code is a MATLAB implementation and is not parallelised. The runtime is therefore not optimal, but the trends are still clear.

Fig. 6 Runtime versus error for 6th, 8th, 10th and 12th order operators

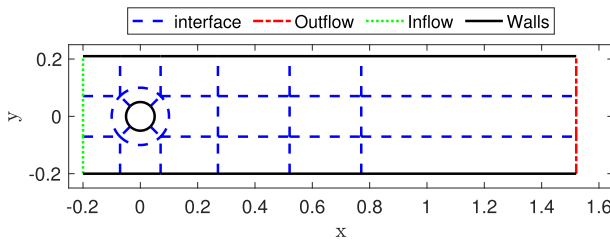
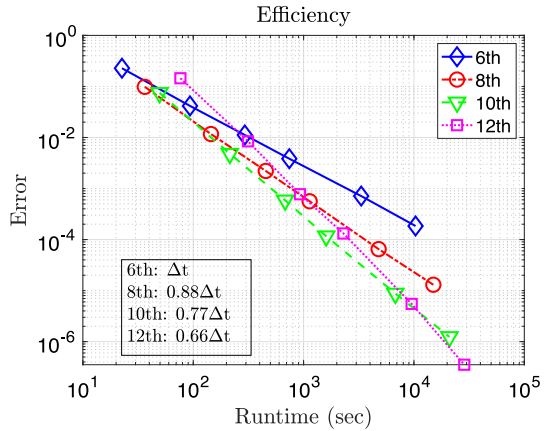


Fig. 7 Multi-block discretisation using 21 blocks for the domain of the cylinder in a flow benchmark computation

5.2 Flow Around Cylinder

A benchmark that is often used for incompressible flow solvers is the flow around a cylinder, referred to as the benchmark 2D-3 in [28]. Accurate reference solutions have been developed in [31]. The domain is a long, thin channel with a circular obstruction inside it. The flow is introduced from the left with an inflow velocity that is sinusoidal in time. For our discretisation, the domain is constructed in a multi-block fashion as seen in Fig. 7, showing the interface locations and boundary types. The simulation is run until $T = 8$.

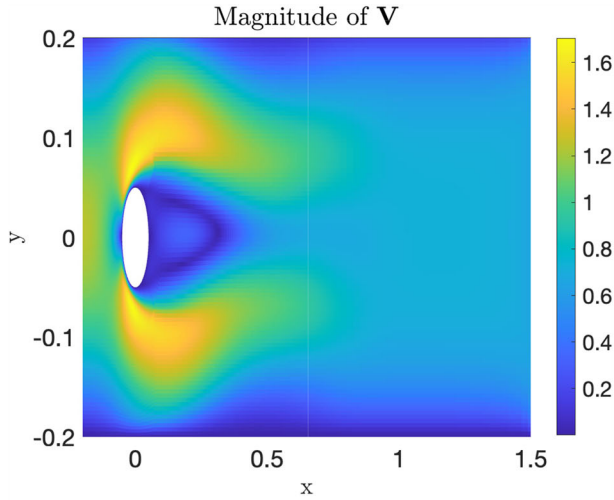
The inflow boundary is set as a Dirichlet BC with an analytic flow profile (57) as data. The outflow boundary is a homogeneous characteristic boundary condition. The upper and lower walls, as well as the circle obstruction, are set as Dirichlet no-slip BC. The interfaces are handled using the projection method to ensure continuity over the blocks.

We elicit a dynamical flow using the flow profile on the inflow boundary

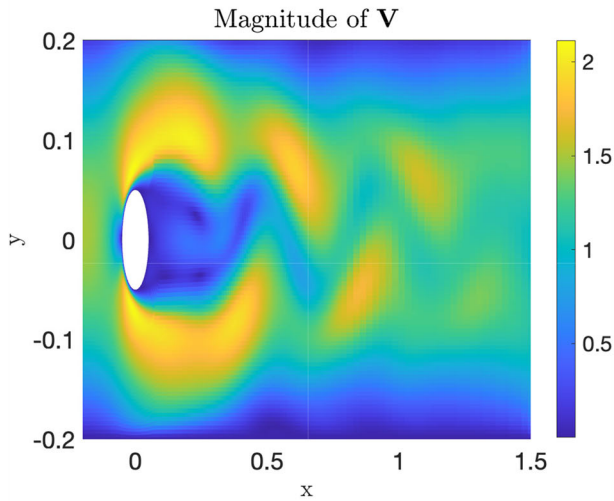
$$u|_{Inflow} = -\sin\left(\frac{\pi}{8}t\right) \frac{6}{0.41^2} (y + 0.2)(y - 0.21). \tag{57}$$

Using the kinematic viscosity $\epsilon = 10^{-3}$, the flow parameters lead to a flow with Reynolds number varying between 0 to 100 over the simulated time.

Remark 4 For $t > 8$ the boundary data in (57) would not constitute an inflow boundary condition anymore, but simply dirichlet boundary conditions for the velocity with negative velocity. Meaning the flow would be going out of the domain at the left boundary. As $t > 8$ this



(a) Snapshot of solution at $T=2.5$, $Re\ 80$



(b) Snapshot of solution at $T=4.2$, $Re\ 100$

Fig. 8 Snapshots of solution at different times, showing different behaviour at different Reynolds numbers. 6th order operator with 22896 DOFs

boundary condition may not be physically relevant, however the imposition of the boundary condition using the projection method is still stable and the solution would be well defined.

As seen in Fig. 8 the flow evolves from laminar to vortex shedding as the Reynolds number of the flow increases over time.

Table 1 Maximum drag and lift coefficient over the simulation time, and difference of pressure at front and back of the cylinder at $T=8$ for the 6th order operator. The benchmark drag, lift and pressure difference values are given in intervals together with a reference value from [4]

Order	DOFs	C_D	C_L	Δp
6th	13125	2.9909	0.45215	-0.0267
	18900	2.9785	0.48244	-0.0394
	22896	2.9736	0.48893	-0.0447
10th	13125	2.9559	0.4839	-0.071
	18900	2.9540	0.4749	-0.069
	Benchm.	[2.93, 2.97]	[0.47, 0.49]	[-0.115, -0.105]
	[4]	2.9509	0.4778	-0.111

To compare the computations to the benchmark data we calculate the lift and drag coefficients on the surface, S of the cylinder:

$$C_L(t) = -\frac{2}{V_M^2 L} \int_S \left(\frac{\partial V_\tau}{\partial \hat{n}} n_x - p n_y \right) ds, \quad (58)$$

$$C_D(t) = \frac{2}{V_M^2 L} \int_S \left(\frac{\partial V_\tau}{\partial \hat{n}} n_y - p n_x \right) ds.$$

Here $V_M = 1$ is the mean velocity of the incoming velocity field, $L = 0.1$ denotes the characteristic length, here the diameter of the cylinder, and V_τ is the normal velocity on the cylinder. We also measure the pressure difference, denoted Δp , on the leftmost and rightmost points of the cylinder at $T = 8$. The normal derivatives and integrals are calculated using the SBP operators and norms.

Figure 9 shows the behaviour of the lift and drag coefficients over time for an increasing number of degrees of freedom. Table 1 shows the results compared to the benchmark using 6th order operators and 10th order operators. The solutions agree well with the benchmark for the coefficients of drag and lift but differ for the pressure difference, Δp . The pressure difference does not seem to have converged for the resolution of the solutions. The handling of the outflow boundary seems to have a strong effect on the pressure solution; further refining the grid would most likely keep the trend of lowering the pressure difference closer to the benchmark value. Increasing the domain length could have a similar effect on the pressure solution. This was not tested due to the large computational resources required. In accordance with the previous result on efficiency, we can also see that the 10th order operators show better agreement with the benchmark than the 6th order operators, while using fewer degrees of freedom.

6 Conclusions

A high-order SBP finite difference method is developed for the velocity-pressure formulation of the incompressible Navier-Stokes equations in two dimensions for curvilinear multi-block discretisations. The method is proven stable using the energy method. The result holds for any scheme with diagonal norm and that fulfills the SBP-property.

The method is evaluated on two problems on multi-block non-cartesian grids: the Taylor-Green vortex flow in a circular domain and a benchmark problem modeling the flow over

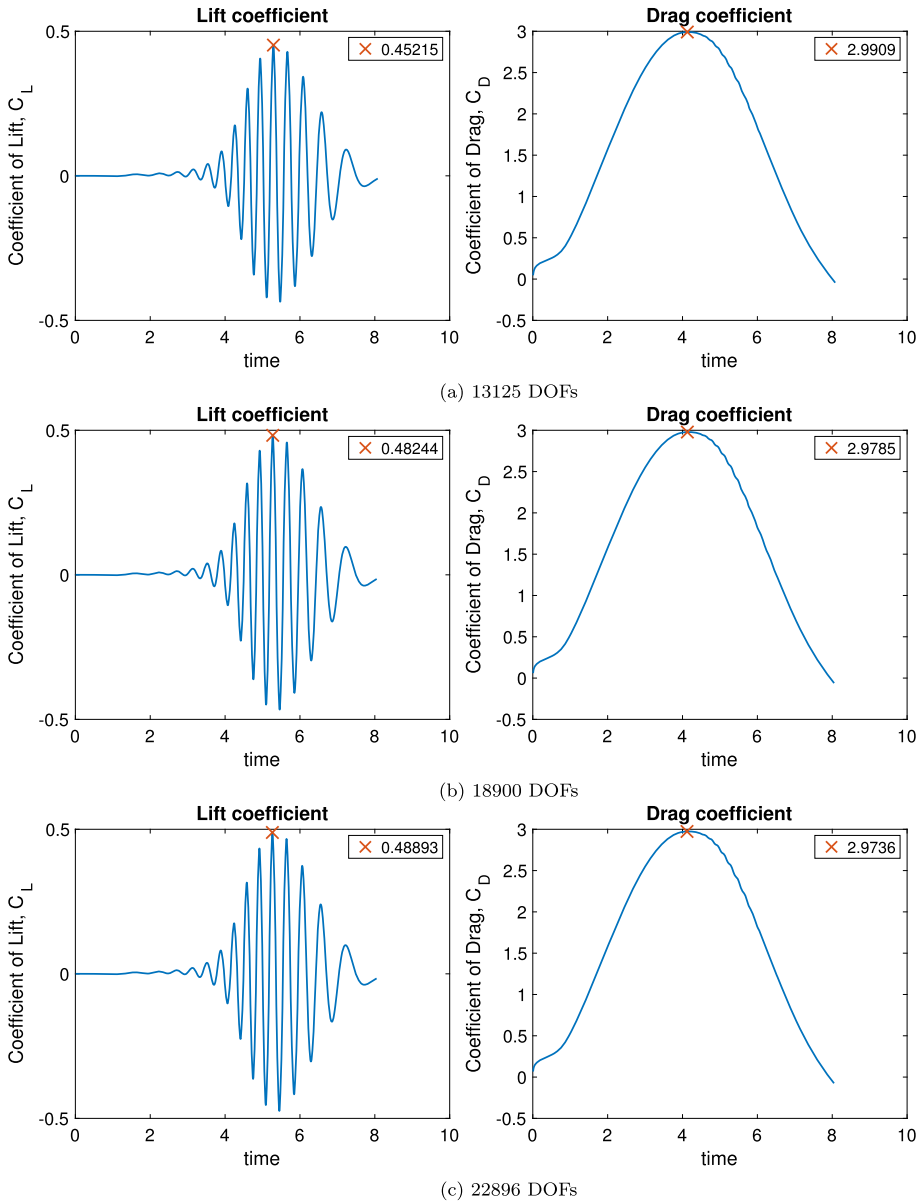


Fig. 9 Lift and drag coefficients over time for the cylindrical obstruction using 6th order operators, with different degrees of freedom

a cylinder. For the Taylor-Green vortex problem, we show that high-order convergence and high-order accuracy are achieved using the scheme. For the more physically relevant benchmark problem, flow over a cylinder, the scheme achieves good agreement with data. In this study, we use boundary optimised SBP-operators of interior order 6, 8, 10, 12. These high-order schemes show increased computational efficiency (accuracy versus computational time) for the Taylor-Green vortex problem as we increase the order of the operators. This

provides a justification and interest for the use of high-order methods, as we can achieve the same accuracy as lower order methods using coarser grids.

The results from the study take steps towards closing the gap between coupling high-order finite difference methods and other discretisation methods for incompressible flow by using the projection method for exact interface couplings using SBP operators. Further extensions would be to extend the scheme to three dimensions and an implementation making use of the highly parallelisable nature of finite difference schemes to speed up the computations.

Acknowledgements The authors would like to thank the support from the resources provided by the Swedish National Infrastructure for Computing (SNIC) at UPPMAX.

Author Contributions David Niemelä: Writing - review & editing, Writing - original draft, Visualization, Software, Methodology, Investigation. Gustav Eriksson: Writing - review & editing, Methodology, Conceptualization. Ken Mattsson: Writing - review & editing, Methodology, Conceptualization.

Funding Open access funding provided by Uppsala University. Open access funding provided by Uppsala University. The work has been supported by the Swedish Research Council (VR) through the project 2021-05830_VR.

Data Availability Enquiries about data availability should be directed to the authors.

Declarations

Conflicts of Interest The authors have no conflicts of interest to declare that are relevant to the content of this article.

Open Access This article is licensed under a Creative Commons Attribution 4.0 International License, which permits use, sharing, adaptation, distribution and reproduction in any medium or format, as long as you give appropriate credit to the original author(s) and the source, provide a link to the Creative Commons licence, and indicate if changes were made. The images or other third party material in this article are included in the article's Creative Commons licence, unless indicated otherwise in a credit line to the material. If material is not included in the article's Creative Commons licence and your intended use is not permitted by statutory regulation or exceeds the permitted use, you will need to obtain permission directly from the copyright holder. To view a copy of this licence, visit <http://creativecommons.org/licenses/by/4.0/>.

References

1. Strikwerda, J.C., Lee, Y.S.: The accuracy of the fractional step method. *SIAM J. Numer. Anal.* **37**(1), 37–47 (1999)
2. Kim, J., Moin, P.: Application of a fractional-step method to incompressible navier-stokes equations. *J. Comput. Phys.* **59**(2), 308–323 (1985)
3. Nguyen, N.C., Peraire, J., Cockburn, B.: An implicit high-order hybridizable discontinuous galerkin method for the incompressible navier-stokes equations. *J. Comput. Phys.* **230**(4), 1147–1170 (2011)
4. Fehn, N., Wall, W., Kronbichler, M.: On the stability of projection methods for the incompressible navier-stokes equations based on high-order discontinuous galerkin discretizations. *J. Comput. Phys.* **351**, 06 (2017)
5. Strand, B.: Summation by parts for finite difference approximations for d/dx . *J. Comput. Phys.* **110**(1), 47–67 (1994)
6. Del Rey, D.C., Fernández, J.E., Hicken, and David W. Zingg.: Review of summation-by-parts operators with simultaneous approximation terms for the numerical solution of partial differential equations. *Computers & Fluids* **95**, 171–196 (2014)
7. Svård, M., Nordström, J.: Review of summation-by-parts schemes for initial-boundary-value problems. *J. Comput. Phys.* **268**, 17–38 (2014)

8. Stiernström, V., Almquist, M., Mattsson, K.: Boundary-optimized summation-by-parts operators for finite difference approximations of second derivatives with variable coefficients. *J. Comput. Phys.* **491**, 112376 (2023)
9. Carpenter, M.H., Gottlieb, D., Abarbanel, S.: Time-stable boundary conditions for finite-difference schemes solving hyperbolic systems: Methodology and application to high-order compact schemes. *J. Comput. Phys.* **111**(2), 220–236 (1994)
10. Mattsson, K., Nordström, J.: High order finite difference methods for wave propagation in discontinuous media. *J. Comput. Phys.* **220**(1), 249–269 (2006)
11. Mattsson, K., Svård, M., Carpenter, M., Nordström, J.: High-order accurate computations for unsteady aerodynamics. *Computers & Fluids* **36**(3), 636–649 (2007)
12. Eriksson, G.: Non-conforming interface conditions for the second-order wave equation. *J. Sci. Comput.* **95**, 6 (2023)
13. Gassner, G. J.: A skew-symmetric discontinuous galerkin spectral element discretization and its relation to sbp-sat finite difference methods. *SIAM Journal on Scientific Computing*, 35, (2013)
14. Wang, S., Kreiss, G.: A finite difference-discontinuous galerkin method for the wave equation in second order form. *SIAM J. Numer. Anal.* **61**(4), 1962–1988 (2023)
15. Eriksson, G., Mattsson, K.: Weak versus strong wall boundary conditions for the incompressible navier-stokes equations. *J. Sci. Comput.* **92**, 07 (2022)
16. Almquist, M., Dunham, E.M.: Non-stiff boundary and interface penalties for narrow-stencil finite difference approximations of the laplacian on curvilinear multiblock grids. *J. Comput. Phys.* **408**, 109294 (2020)
17. Malvern, L. E.: Introduction to the mechanics of a continuous medium. (1969)
18. Mattsson, K.: Summation by parts operators for finite difference approximations of second-derivatives with variable coefficients. *J. Sci. Comput.* **51**(3), 650–682 (2012)
19. Svård, M.: On coordinate transformations for summation-by-parts operators. *J. Sci. Comput.* **20**(1), 29–42 (2004)
20. Mattsson, K.: Summation by parts operators for finite difference approximations of second-derivatives with variable coefficients. *J. Sci. Comput.* **51**(650–682), 6 (2012)
21. Mattsson, K., Nordström, J.: Summation by parts operators for finite difference approximations of second derivatives. *Journal of Computational Physics - J COMPUT PHYS* **199**(503–540), 09 (2004)
22. Nordström, J., Mattsson, K., Swanson, C.: Boundary conditions for a divergence free velocity-pressure formulation of the navier-stokes equations. *J. Comput. Phys.* **225**(1), 874–890 (2007)
23. Kreiss, H.-O., Lorenz, J.: *Initial-Boundary Value Problems and the Navier-Stokes Equations*. Society for Industrial and Applied Mathematics, (2004)
24. Nordström, J.: Nonlinear boundary conditions for initial boundary value problems with applications in computational fluid dynamics. *J. Comput. Phys.* **498**, 2 (2024)
25. Nordström, J.: Open boundary conditions for nonlinear initial boundary value problems. *J. Comput. Phys.* **530**, 6 (2025)
26. Olsson, P.: Summation by parts, projections, and stability. I. *Mathematics of Computation* **64**(1035–1065), 07 (1995)
27. Mattsson, K., Olsson, P.: An improved projection method. *J. Comput. Phys.* **372**, 349–372 (2018)
28. Schäfer, M., Turek, S., Durst, F., Krause, E., Rannacher, R.: *Benchmark Computations of Laminar Flow Around a Cylinder*, pages 547–566. Vieweg+Teubner Verlag, Wiesbaden, (1996)
29. Gustafsson, B., Kreiss, H.-O., Sundström, A.: Stability theory of difference approximations for mixed initial boundary value problems. II. *Mathematics of Computation* **26**(119), 649–686 (1972)
30. Svård, M., Nordström, J.: On the convergence rates of energy-stable finite-difference schemes. *J. Comput. Phys.* **397**, 11 (2019)
31. John, V.: Reference value for drag and lift of a two-dimensional time dependent flow around cylinder. *Int. J. Numer. Meth. Fluids* **44**(777–788), 03 (2004)